Title: Tuning the electronic properties of a clean TiO2(1 1 0) surface via repeated sputtering and annealing: A KPFM and LC-AFM study

Author: K. Cieślik, D. Wrana, K. Szajna, W. Bełza, M. Rogala, Krzysztof Szot [i in.]

Citation style: Cieślik K., Wrana D., Szajna K., Bełza W., Rogala M., Szot Krzysztof [i in.]. (2022). Tuning the electronic properties of a clean TiO2(1 1 0) surface via repeated sputtering and annealing: A KPFM and LC-AFM study. "Applied Surface Science" (2022), vol. 571, s. 1-9, art. no. 151303. DOI: 10.1016/j.apsusc.2021.151303

Applied Surface Science 571 (2022) 151303

Contents lists available at ScienceDirect

Applied Surface Science

journal homepage: www.elsevier.com/locate/apsusc

Full Length Article

Tuning the electronic properties of a clean TiO_2(1 1 0) surface via repeated sputtering and annealing: A KPFM and LC-AFM study

K. Cieślik [a,*], D. Wrana [a], K. Szajna [a], W. Bełza [a], M. Rogala [b], C. Rodenbücher [c], P. Dąbczyński [a], K. Szot [d,e], F. Krok [a]

[a] Marian Smoluchowski Institute of Physics, Jagiellonian University, Krakow 30-348, Poland
[b] Faculty of Physics and Applied Informatics, University of Lodz, Pomorska 149/153, 90-236 Lodz, Poland
[c] Institute of Energy and Climate Research (IEK-14), Forschungszentrum Jülich, 52425 Jülich, Germany
[d] August Chelkowski Institute of Physics, Silesian University, Katowice, Poland
[e] aixACCT Systems GmbH, 52068 Aachen, Germany

A B S T R A C T

Repeated sputtering and annealing are standard preparation methods for obtaining a stoichiometric TiO_2(1 1 0) surface for surface science experiments. However, both processes result in a reduction in TiO_2 crystal when used separately, leading to the modification of the physical and chemical properties of oxide materials. Our investigation aims to determine how these two processes affect the electronic properties of the surface and subsurface regions at the nanometer scale. To accomplish this goal, we utilized local microscopy (Kelvin probe force microscopy and local-conductivity atomic force microscopy) and spectroscopy methods (X-ray photoelectron spectroscopy and secondary ion mass spectrometry). We found that repeated sputtering and annealing does, in fact, affect both the conductivity and work function of the surface. The work function, as well as conductivity, increase with increasing number of cycles, but then reach a plateau. Furthermore, we show that the way the surface is prepared, using multiple cycles or one cycle of equivalent ion-beam fluence, matters. We attribute the differences in the crystal properties to the dynamics of stoichiometric changes during sputtering and subsequent annealing which we illustrate using secondary ion mass spectroscopy, which shows that after multiple cycles the subsurface layer is modified, even though XPS shows a stoichiometric surface.

1. Introduction

Rutile titanium dioxide is one of the most widely-studied oxide materials, with applications ranging from photocatalysis [1], memristors [2], solar cells [3,4], sensors [5], and thin-film MOS transistors [6], to antibacterial additives for denim fabrics [7]. With so many applications, it is not surprising that basic research aimed at better understanding the processes that give rise to the versatility of the applications is also increasing. To understand the processes that are the basis of such applications, controlled conditions are required, and investigations into the surfaces of monocrystals in ultra-high vacuum conditions can provide such needed model systems. Such studies can deliver an entirely new perspectives and contribute to the understanding and development of applications, as is the case, e.g., with photocatalysis [8]. However, obtaining a suitable surface that can be used in such investigations is not trivial and many different methods for obtaining atomically-flat and stoichiometric surfaces exist. One of the most utilized preparation methods is that of repeated sputtering and annealing.

The sputtering-annealing of cleaning cycles to obtain atomically flat surfaces with well-developed terraces is a time-tested method used in most laboratories. In the literature, there are a variety of procedure that rely on repeated sputtering by low energy (from 0.6 keV [9], through 1 keV [10,11] to 2 keV [12,13]) noble ion beams (Ar^+ [9], Ne^+[14,15]), followed by annealing at high temperatures (from 800 K [16,12] through 1000 K [11,17] to even 1200 K [9]). These cleaning cycles have become the standard, non-destructive way of preparing a TiO_2 surface. However, there is no set procedure with strict parameters that must be followed in order to obtain the desired surface using cleaning cycles. The experimental details, such as the temperature, time and fluence used during preparation vary across different studies. Moreover, some studies do not even contain details of the preparation procedure, e.g., the energy of the ions used in sputtering [18,19,20]. The common denominator is the fact that such cleaning cycles are performed until a sharp diffraction (1×1) pattern is observed using low-energy electron diffraction (LEED), and no contamination is detected using either x-ray photoelectron spectroscopy (XPS) [21] or Auger spectroscopy [22]. Alternative methods are of course also used, such as some that forego sputtering in favour of etching in HF acid and an increase in the annealing

* Corresponding author.
E-mail address: karol.cieslik@doctoral.uj.edu.pl (K. Cieślik).

https://doi.org/10.1016/j.apsusc.2021.151303
Received 31 May 2021; Received in revised form 1 September 2021; Accepted 13 September 2021
Available online 24 September 2021

temperature [23]; however, cleaning cycles still seem to dominate surface science investigations into TiO_2(1 1 0).

However, both components (processes) of the cleaning cycle lead to changes in the oxide crystal – its chemical compositions and properties. By its nature, sputtering with an ion beam causes a reduction in the TiO_2 crystal via the preferential sputtering of oxygen atoms [24], which significantly changes the electrical conductivity of the surface [25]. Furthermore, the higher the energy of the projectile ions used, the greater is the rate of reduction during sputtering [26]. Similarly, annealing causes thermal reduction, which can even be observed by monitoring the crystal's mass loss [27] or simply by measuring the oxygen signal during annealing using a mass spectrometer [28]. Thus, at their core both processes feature the loss of oxygen from the crystal, with each oxygen molecule leaving behind two electrons and an oxygen vacancy that affects the crystal's electronic properties.

The reduction of TiO_2 during typical sputtering-annealing cleaning cycles procedure is not a minuscule effect. Quite the opposite, the entire crystal changes colour from transparency to a bluish hue [9]. Moreover, the crystal's thermal reduction increases its electrical conductivity by orders of magnitude [29]. The changes in properties are linked to changes in the composition of the TiO_2 crystal, with a thermogravimetric analysis showing a mass loss of 0.05% for TiO_2 annealed in 800 °C after approximately 10 h in reducing conditions [30]. Such mass loss can be associated with the formation of a wide range of extended defects and even structural changes in the TiO_2 to Magnéli phases [30]. Both ion beam-induced reduction and the thermal reduction of oxides are, by their nature, surface processes which, when coupled to the drastic observed macroscopic changes, raise the question of the changes in surface properties that occur during such a preparation method.

In order to investigate the changes in the electronic properties of sputtering–annealing cleaning cycles prepared on a TiO_2 surface, Kelvin Probe Force Microscopy (KPFM) and Local-Conductivity Atomic Force Microscopy (LC-AFM) were used, as both of these methods enable "local" in-situ investigations to be carried out, even at the atomic scale (for LC-AFM [31] and KPFM [32,33]). KPFM is a method for mapping the work function. It has been successfully used to investigate many phenomena, ranging from studies of Fermi energy level pinning [34] and the comprehensive characterization of solar cells [35], to studies on an atomic scale, such as the adsorption of O_2 on TiO_2 [32]. LC-AFM allows for measurements of the surface conductivity, and has been used extensively to investigate resistive switching in thin films of TiO_2 ([36,37,38]), as well as crystals [39,40]. LC-AFM has also been used, e.g., to observe the photoelectric switching on the interface of WO_3/TiO_2 films [41]. Both of these techniques show great synergy when used together, either when resistive switching is observed ([42,39,36,37]) or when only redox processes are concerned [43,44], or when information about electronic properties is needed to characterize materials ([45]) or their decay [46].

The aim of this study was to determine how repeated sputtering and annealing influences the electronic properties and chemical composition of TiO_2(1 1 0). Some findings reported in the literature indicate the increase in the work function of rutile after multiple cycles [47], but it has not been studied systematically and only the trend has been indicated, with no values. With respect to the effect of sputtering and annealing on the conductivity of TiO_2(1 1 0), the effects of these processes were separately studied (thermal annealing: [39]; sputtering: [25]), whereas the combined effect of the cycles on this property, to the best of the authors' knowledge, has not been studied thus far. In order to analyze and understand how these processes affect the electronic properties of the TiO_2(1 1 0) surface, KPFM and LC-AFM were used with the addition of XPS and secondary ion mass spectrometry (SIMS) measurements. XPS and SIMS enabled us to clearly show the drastic changes in stoichiometry during a single cleaning cycle (from high surface non-stoichiometry after sputtering to stoichiometry after annealing), as well as to demonstrate that multiple cycles lead to changes in the stoichiometry of the crystal subsurface region. These compositional changes also impact the electronic properties, which demonstrates that repeated sputtering and annealing may be used as methods for altering and tailoring these properties, depending on the outcome desired.

2. Experimental

2.1. Sample preparation

The rutile monocrystals of an epi-ready, one-side-polished TiO_2(1 1 0) surface were provided by Shinkosha (Japan). The samples were mounted on silicon wafers and introduced to ultra-high vacuum (UHV) systems with a base pressure of 5.0E-10 mbar. After degassing for 15 min at 300 °C, depending on the specific experiment's goal, they underwent different regimes of sputtering with Ar^+ ions at RT and annealing at 800 °C. The samples were annealed by direct heating with an AC current method in order to avoid non-uniform crystal reduction due to ionic current flow [48]. As for the sputtering process, a low-energy (2 keV) Ar^+ ion beam (of few mm in diameter) with an average ion beam flux of 1.0E13 ions cm^{-2} s^{-1} was rastered over the sample at an angle of 30° with respect to the normal surface direction.

The first set of experiments aimed to determine how multiple sputter-annealing cleaning cycles (CCs) affect the physicochemical properties of the TiO_2(1 1 0) surface. The surface was subjected to cycles consisting of sputtering with Ar^+ ions (RT, fluence 8.61E15 ions cm^{-2}) and annealing at 800 °C for 15 min. The properties of the sample were measured after 1, 5, 10, 15, 20, 25, 30, 35, 40, and 50 CC. After the total of 50 CC, the cumulative fluence was equal to 4.3E17 ions cm^{-2} and the total annealing time was 13 h and 30 min. As the last step in the investigation, the sample was oxidized with isotopic $^{18}O_2$ gas, first at room temperature, with oxygen exposure up to 1900 L, followed by oxidation at an elevated sample temperature of 800 °C for 1 h and oxygen partial pressure of 5E-8 mbar. The sample underwent SIMS profiling to check the content of the ^{18}O in the processed subsurface region. It was compared to an as-received crystal which was only annealed in isotopic oxygen at 800 °C for 1 h.

The second experiment's goal was to investigate, separately, the influence of ion beam fluence on the changing of the conductivity, work function and sample morphology, and how the subsequent process of annealing affects these properties. For this experiment a new monocrystal was used. First, the sample was outgassed at 800 °C for one hour in order to desorb the organic adsorbates. Then, the sample was non-uniformly sputtered at RT (i.e., with increasing fluence along with one of the sample surface directions) with the ion beam fluence ranging from 5.0E15 to 1.2E17 ions cm^{-2}. After the measurements, the sample was annealed at 800 °C for one hour. Another monocrystal was prepared for KPFM investigations by first outgassing at 800 °C and then sputtering at RT (with three regions of different ion fluence: 5.0E16, 1.2E17, and 3.0E17 ions cm^{-2}) and subsequently annealed at 800 °C for one hour.

Additional samples were prepared for the SIMS investigations – three monocrystals: one which was only sputtered (1.7E17 ions cm^{-2}), one which was sputtered (6.0E16 ions cm^{-2}) and annealed at 800 °C for 1 h, and another one which underwent 11 cleaning cycles– each cycle consisted of sputtering of fluence of 2.0E16 ions cm^{-2} and annealing at 800 °C for 15 min (cumulative fluence 2.2E17 ions cm^{-2} and total annealing time 2 h 45 min). Additionally, the purity of the monocrystals was checked using this method (see Figure S5 in Supplementary Information), as the presence of impurities in oxides is a widely-known problem.

As for the chemical composition of the processed TiO_2(1 1 0) surface, X-ray photoelectron spectroscopy (XPS) experiments were performed. For this purpose, the surface was subjected to cycles similar to those for the first experiment described above. Three CCs were performed with XPS measurements after each step, each cycle consisted of sputtering of fluence approx. 8E15 ions cm^{-2} and annealing at 800 °C for 15 min.

2.2. Experimental techniques

The scanning probe measurements were performed using an Omicron UHV-RT STM/AFM microscope. The STM imaging was conducted with a positive sample bias of 1.5 V, using a chemically-etched tungsten tip. The LC-AFM measurements were performed at sample biases ranging from 10 mV to 200 mV, depending on the specific sample's conductivity. For both the contact (LC-AFM) and non-contact (KPFM) modes, the same PPP-contPt cantilevers were used (Pt-Ir coated, eigenfrequency: 17 kHz). The KPFM imaging was undertaken using a single pass method that used three separate feedback loops (amplitude, frequency and bias) [49]. In order to operate in non-contact mode, the cantilever was excited to higher harmonics (approximately 90 kHz). The cantilever's oscillation amplitude was approximately 10 nm, whereas the modulation sample bias frequency was in the range of 100–200 Hz and its amplitude of 500 mV was used. For the evaluation of the absolute work function of the measured samples, the KPFM cantilevers were calibrated against the HOPG surface with the assumed work function of 4.5 eV [34,50] before and after each CPD measurement. This calibration procedure was repeated after each KPFM measurement in order to compensate for a possible tip modification during scanning (the variation of the CPD values throughout the experiment is depicted in Figure S1 in Supplementary Information).

A secondary ion mass spectrometer TOF SIMS V (Munster, Germany) equipped with a bismuth manganese liquid metal ion source and Cs ion source, was used to investigate depth profiles of the samples. The profiles were collected in dual beam interlaced mode. 1 keV Cs^+ ion beam was used to sputter over 350 × 350 μm^{-2} area and 30 keV Bi^+ ion beam (100 × 100 μm^{-2} area) concentric to the sputtered surface. Depth calibrations were obtained based on respective crater depth measured with the stylus profilometer (DektakXT Bruker).

The XPS measurements were performed on a Phoibos 150 (SPECS) spectrometer with a 2D-CCD detector. A DAR 400 X-ray lamp with non-monochromatic radiation of 1253.64 eV (Mg Kα) was utilized.

3. Results

Fig. 1a displays the STM morphology after successive sputtering–annealing cycles (CCs). The surface is composed of atomic terraces of tens of nm in width, separated by monoatomic steps of 3.2 Å in height. With the increasing number of CCs, the terrace edges became more compact, and the terraces are becoming wider and have fewer monoatomic in-depth pits. LEED measurements exhibit a typical (1 × 1) pattern after each checked CC (for example, see the insert of Fig. 1a), which indicates that the surface is stoichiometric, as the heavily reduced rutile (1 1 0) crystals are supposed to display a (1 × 2) reconstruction [51,52]. The high-resolution STM images (Fig. 1d, e) show the TiO_2(1 1 0) surface with the (1 × 1) morphology consisting of anisotropic atomic rows running along a [0 0 1] surface direction. All of the STM images were collected with a positive bias, yet the images in Fig. 1d, e present the surface in a different manner. This is because during scanning, the tungsten tip modified itself, which led to different orbitals being exposed at the tip's apex. Such STM tip-apex changes may even lead to drastic changes in the collected image (even contrast inversion) [53]. The STM topography in Fig. 1d reflects the TiO_2(1 1 0) empty states (the positive sample bias), with bright rows originating from the Ti^{4+} atoms between the dark oxygen-bridge rows [54]. The bright spots in Fig. 1e (such as the one marked with "A") show hydroxyl groups. We calculated the coverage based on 20 nm by 20 nm images, for 20, 30 and 40 CC we obtained hydroxyl coverages of respectively 13, 13, 11 % ML. In contrast, it was reported that this density could depend on a number of CCs and ranges from 2.5% ML for nine cycles to 6.1% ML for 32 [55]. Moreover, coverages with point defects of 8% [56] and 15% [57] have also been reported after multiple cycles. Based on the STM images, we can conclude that even though the LEED diffraction patterns show well-defined spots of the (1 × 1) pattern, the surface contains point defects. However, the observed concentration of defects does not allow for unambiguous detection via the XPS measurements. The XPS analysis (Fig. 1c) confirms that the surface is in stoichiometric form (with Ti^{4+} charge state) following the heating. Additionally, the cleaning cycles

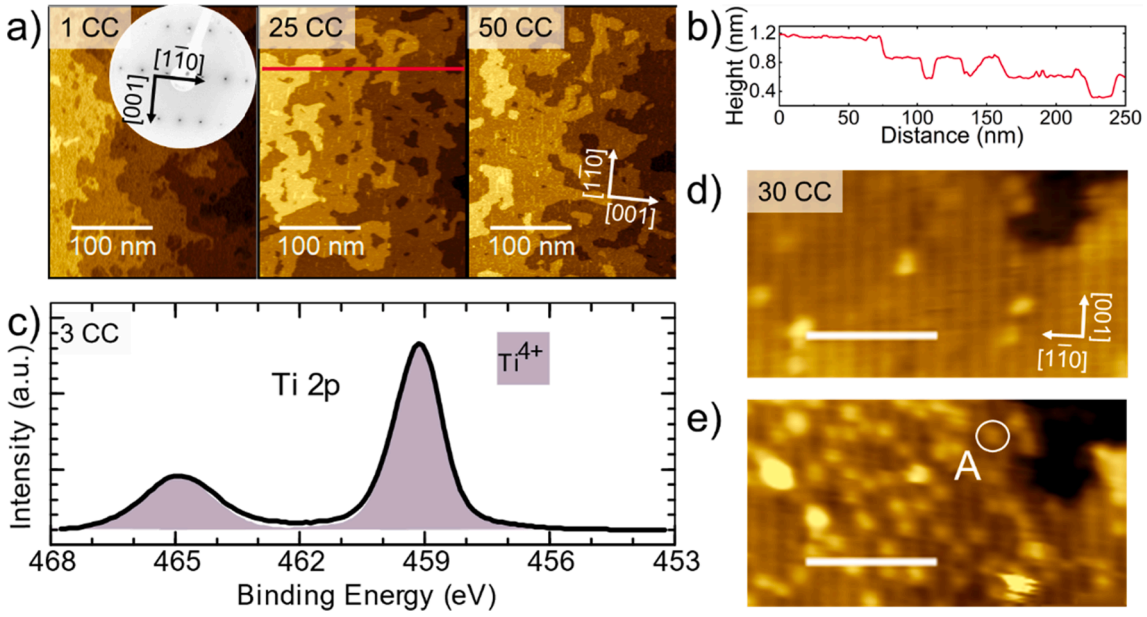

Fig. 1. a) STM morphology and crystallography of the TiO_2(1 1 0) surface that underwent repeated sputtering and annealing (referred to as the cleaning cycles [CCs]) with a LEED insert, high-resolution STM images; b) the line profile through the terraces from the red line on the STM image for 25 CC d), e) showing the surface after 30 CCs imaged using the same tungsten tip, which changed during image acquisition (its orientation, composition, structure or tip apex atom might have changed), the surface structure label "A" refers to the OH– defect, whereas the white scale bar represents 5 nm; and c) XPS spectrum of the TiO_2(1 1 0) that underwent 3 CCs. The doublet of Ti^{4+} states at energies of 459.2 and 465.0 eV can be clearly seen. LEED images were taken using electrons of energy 106 eV, whereas the STM images were acquired using a tunnelling current of approximately 20 pA and a + 1.75 V sample bias. (For interpretation of the references to color in this figure legend, the reader is referred to the web version of this article.)

affect the macroscopic (optical) properties of the TiO_2 crystal, as it changes colour, from being transparent to a bluish hue. Furthermore, this cleaning procedure, which combines two reducing processes, affects other properties of the crystal, such as the crystal conductivity or the work function of its surface.

We performed 50 CCs and, after every fifth, monitored the surface morphology development and its conductivity and work function changes using the LC-AFM and KPFM techniques, respectively. Fig. 2a and b show work function maps, morphology, and local-current maps of TiO_2(1 1 0), collected with the same AFM tip after the 10th and 50th cycles. The surface of the as-received TiO_2(1 1 0) crystal is insulating, and is becoming conductive with subsequent initial cleaning cycles. Then, the sample conductivity starts to saturate for a large number of cycles, as is shown in Fig. 2c. In the current maps (see Fig. 2a and b), the conductivity signal exhibits an inhomogeneous structure and does not appear to be directly related to surface features. For the initial cycles, the conductivity is more grain-like structure, and the surface became more homogeneous in terms of conductance in the later stage of cleaning. The insert of Fig. 2c shows a change in the I-V characteristic, from rectifying to ohmic behavior, for an increasing number of cycles. It clearly demonstrates that the surface became more metallic-like in what can be related to an insulator-to-metal transition.

Similarly, as with the conductivity, the work function of the cleaned TiO_2(1 1 0) surface increases with the increasing number of cleaning cycles, as is shown in Fig. 2d. However, it reaches a plateau with a value of 4.8(1) eV. Closer inspection of the signal variation in the work function maps reveals no correlation with the surface morphology features. The increase in the work function with increasing numbers of cleaning cycles has also been observed [47], although a value for the TiO_2(1 1 0) rutile has not been explicitly specified.

The STM, LEED and XPS results, as noted above, reveal that the TiO_2(1 1 0) surface, even after many CCs, is virtually stoichiometric. Still, the changes in the electrical conductivity of the sample indicate that the subsurface region may have significantly changed. This assumption is entirely justified if one considers that, firstly, the bombardment with the ion beam, in addition to modifying the surface morphology of the sample, entails compositional changes to a depth corresponding to a projectile penetration range of a few nm, as reported in the literature [59]. The progressive depletion of oxygen in TiO_2 during ion bombardment can, in some cases, even induce the formation of new phases [60]. Secondly, thermal annealing is also associated with the ion vacancies diffusion in the subsurface region of the TiO_2 crystal which could be a complex process [61,62]. Indeed, the measured SIMS depth profiles exhibit the major impact of the CCs on the TiO_2(1 1 0) subsurface layer's chemical composition. Fig. 3a shows the SIMS depth profiles of three monocrystals – one which was only sputtered, one which was sputtered and annealed, and another one after 11 cycles. It can be clearly seen that the highest non-stoichiometry is present for the subsurface region of the sample, which was only sputtered. The raw SIMS profiles show that the subsurface layer, in terms of non-stoichiometry and depth of occurrence, is approximately the same for samples that underwent one cycle and 11 cycles. The non-stoichiometry can be seen at depths of up to about 8 nm, deeper than that of the penetration of argon ions during sputtering. It should be noted that the measured $CsO^+/CsTi^+$ ratio does not reflect the sample stoichiometry in the bulk, but this is not surprising, as such divergences have been seen before in the case of the SIMS profiles of TiO_2 crystals [63]. We assume that the ratio of approximately 0.8, seen at depths of tens of nanometers corresponds to stoichiometric ratio.

In order to further investigate the changes introduced by the

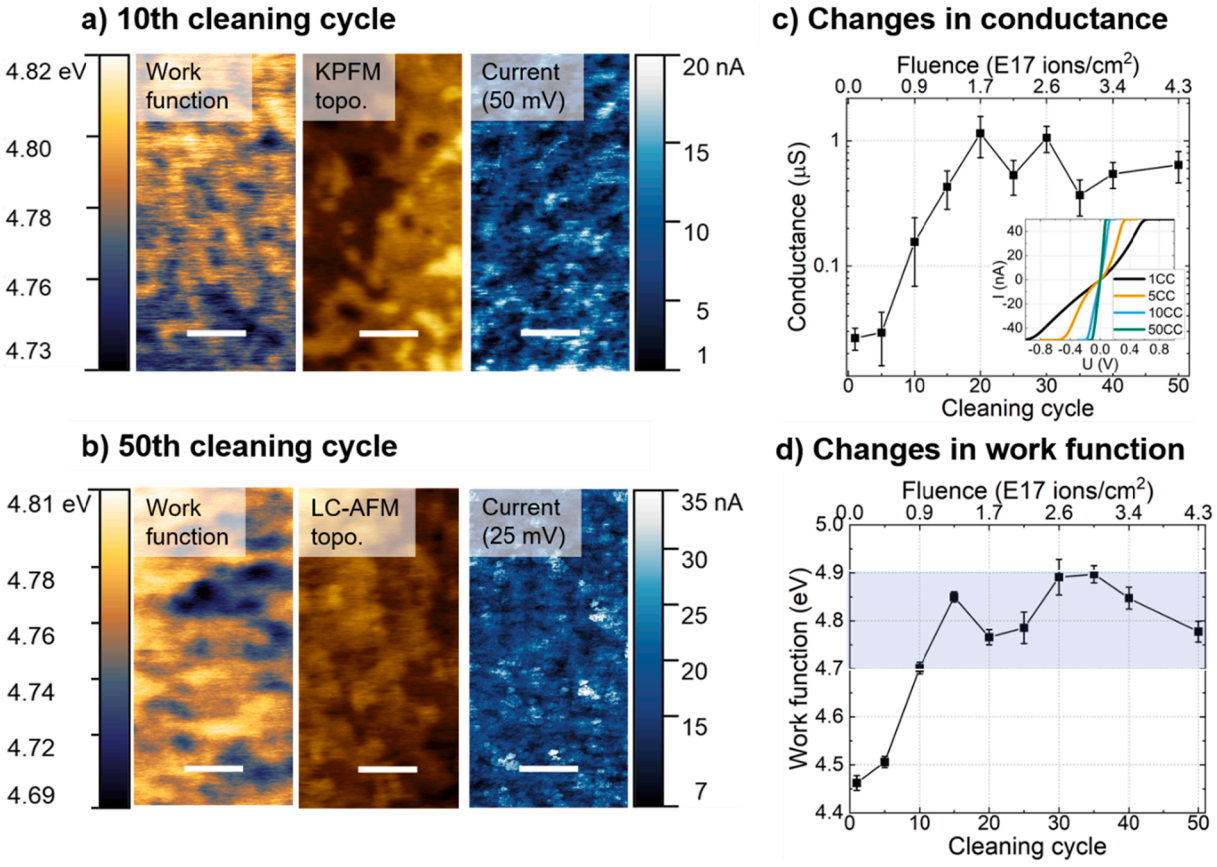

Fig. 2. The work function, topography, and current maps for: a) 10th cleaning cycle (10CC); and b) the 50th cleaning cycle (50CC) – the white scale bar corresponds to 100 nm. The effect of the multiple cleaning cycles on the surface conductance and work function of TiO_2(1 1 0) is shown in c) and d), respectively. The insert in c) shows the selected I-V curves. The work function, as well as the conductance, was calculated based on 500 nm by 500 nm images.

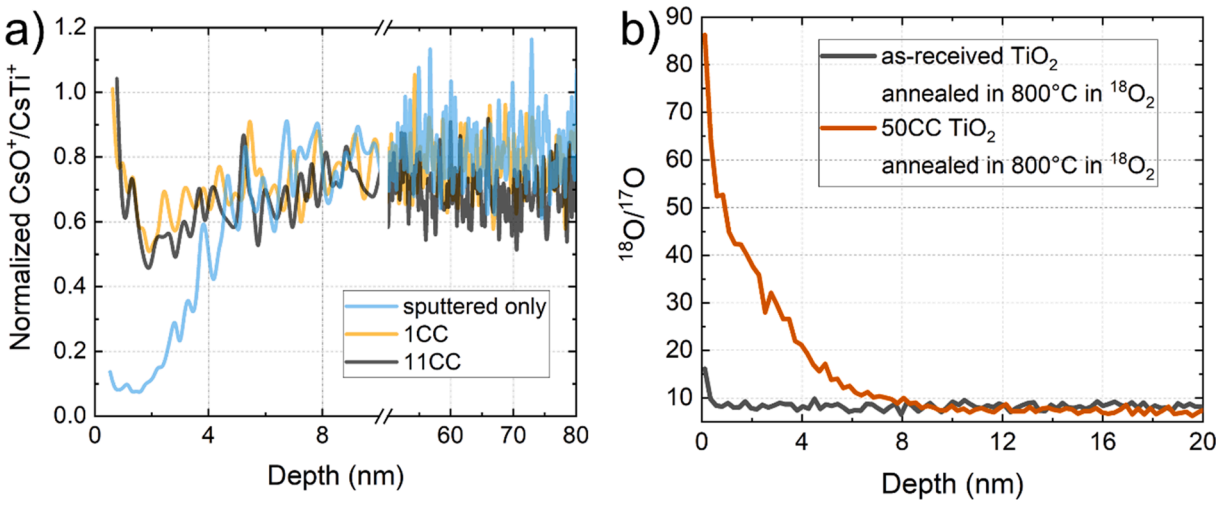

Fig. 3. a) The SIMS depth profiles of the oxygen-to-titanium ratio normalized to an "as received" sample. The measured signals used CsO^+ and $CsTi^+$, as such clusters exhibit a lower matrix effect than O^+ and Ti^+ [58]; b) the SIMS profiles for two samples annealed in isotopic oxygen: one which underwent 50 CCs prior to this procedure and the other, as-received sample which did not undergo the CCs. ^{17}O was used as a reference instead of the more abundant ^{16}O, as its concentration is also constant in the crystal and it does not overwhelm the detector.

analyzed processes in the subsurface region of a TiO_2 crystal, we performed an experiment in which we compared the isotopic oxygen content in the subsurface regions of "50 CC" and "as received" TiO_2(1 1 0) samples annealed in isotopic ^{18}O. Seebauer et al. have already shown that oxygen-rich conditions combined with high temperatures can lead to the injection of oxygen interstitials and the subsequent annihilation of oxygen vacancies in the crystal [64,65]. The resulting SIMS profiles, shown in Fig. 3b, clearly indicate that performing 50 CCs on a sample alters the crystal. The depth of penetration of the oxygen isotope is significantly higher than that for the reference sample (up to 10 nm compared to almost no signal for the reference sample).

In order to determine if changes in the properties after multiple cycles are reversible and learn more about the defects present in this crystal, we oxidized the 50 CC TiO_2(1 1 0) crystal at RT. As is depicted in Fig. 4a, oxidation at room temperature decreases the conductivity. The conductance histograms (Fig. 4b) show that not only the value of the conductance changes but also its distribution – with oxidized surfaces showing a more compact and symmetrical distribution of conductance. Such changes in the conductivity of the TiO_2 surfaces oxidizing at RT were also observed for annealed-only TiO_2(1 1 0) [39]. It is well-established that exposure to molecular oxygen at temperatures greater than 100 K restores the stoichiometry of the TiO_2(1 1 0) surface [66], which explains the drop in the conductivity after oxidation at RT. The exposure to oxygen reduced the small percentage of surface defects present on the surface after multiple cleaning cycles, which can be seen in the STM images (Fig. 1b). However, this does not entirely reverse the conductance of the surface to the value at the beginning of the experiments (Fig. 4a) and means that the oxidation at RT does not mitigate the subsurface defects (and not even all of the surface oxygen vacancies [61,67]), which are present in the sputtered and annealed samples [66]. On the other hand, the exposure to oxygen leads to an increase in the work function from a value of 4.8(1) eV to 5.03(8) eV (Fig. 4c). An increase in the work function of oxidised TiO_2 has been observed elsewhere for the annealing in oxygen ([68,69]), where it has been treated with oxygen plasma [47] or exposed to oxygen in RT [68]. When a reduced surface is exposed to oxygen, the oxygen vacancies are filled with oxygen atoms which, in themselves, have a strong electron affinity. This results in a surface with a negative overall surface polarity, leading to an increase in the work function [68]. Our results highlight this increase in the work function, the final value of which was 5.03(8) eV, which is close to the values reported for the surfaces annealed in oxygen, for example 5.3 eV for the UPS measurements [69]. The slight discrepancies could relate to the fact that simple exposure to oxygen does not heal as many oxygen vacancies as annealing of the sample in oxygen.

As the CCs undoubtedly affect the properties of the TiO_2, in order to clarify how the individual processes, i.e., sputtering and annealing, contribute to the observed changes, we performed an experiment in which we performed only one CC for a non-uniformly sputtered sample. The sample was irradiated with increasing ion fluence, along with one of the sample surface directions. In this manner, we could determine how

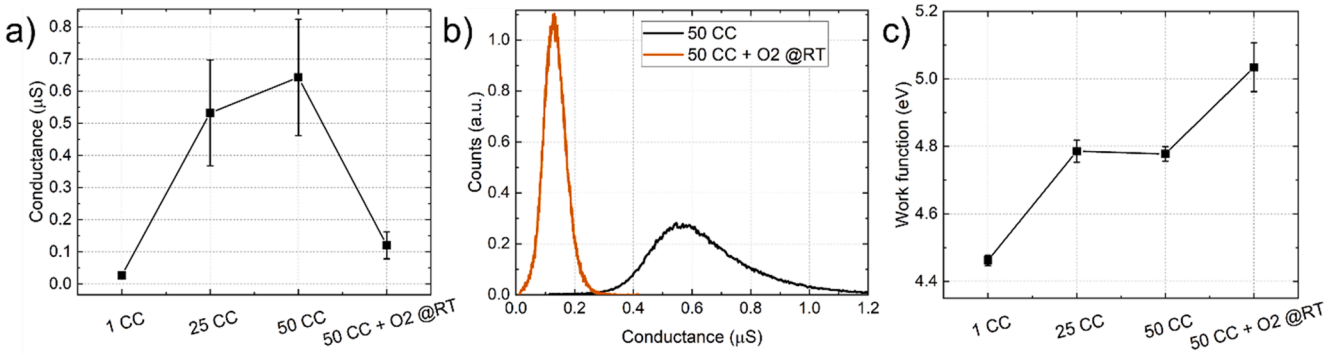

Fig. 4. Changes in the properties of the processed TiO_2(1 1 0) surface prior to and after oxidation at room temperature (310 L for KPFM and 1900 L for LC-AFM), as seen in the graphs and showing changes in the conductance (a) and work function (c). In b) can be seen histograms of the conductance signals from LC-AFM maps.

the surface's properties changed after each step in a cycle and whether these changes were dependent on the ion-beam's fluence. Furthermore, we would answer the question of multiple cycles leading to the same changes in the physicochemical properties of the TiO_2(1 1 0) crystal in terms of a single CC with an equivalent sputtering fluence.

As Fig. 5a shows, sputtering leads to a rough surface with no discernible terraces. Furthermore, the LEED measurements indicate a lack of long-range ordering, as no diffraction spots are present. We also observed that with the increasing ion beam fluence, the surface roughness also increases (from 0.24 nm for the fluence of 7.0E15 ions cm^{-2} to 0.36 nm for 1.2E17 ions cm^{-2}). The conductivity of the sputtered samples exhibits ohmic characteristics (Fig. 5a) and rapidly increases with increasing ion-beam fluence, as is shown in Fig. 5c. The XPS spectrum of the sputtered sample (Fig. 5d) clearly demonstrates that it is far from stoichiometric, with significant additions of Ti^{3+} and Ti^{2+} ions (approximately 35% and 5%, respectively). This is a consequence of the preferential sputtering of oxygen atoms during irradiation of the TiO_2 crystal [24]. The reduction in the crystal, with increasing concentrations of Ti^{2+} and Ti^{3+} ions, implies the formation of oxygen vacancies within the sample structure and new electronic states in its band gap, resulting in the transformation from semiconductor to metal-like material. On the other hand, the sputtered surface has a lower value work function compared to that of the surface with completed sputtering-annealing cycles, as is clearly demonstrated in Fig. 5e. This accords with previous observations, that the work function decreases with increasing defect density on the surface [68].

The experiment above have been performed for ions of energy 2 keV, but based on the work of Hashimoto et al. [70] some deductions can be made on the dependence of ion energy on both, work function and conductance. Using XPS measurements they showed that the equilibrium state that is reached after sputtering depends on the ion energy – the higher energy, the higher non-stoichiometry of the surface. With the increasing ion energy, the surface is more effectively sputtered, both in number of formed ions, as well as their state, as above 100 eV Ti^{2+} ions become apparent in the XPS spectra. Above 1 keV a plateau is reached in the intensity ratio of titanium states. Since the work function is a surface property, we can conclude that sputtering using ions of energies above 1 keV would most likely lead to the same values of this property, but for energies below, the work function might be higher, as the surface would be less reduced. Stoichiometry of the surface is not the only property that is affected by ion energy, as the depth of changes also can be changed. With the increasing projectile energies, the projected range and straggling of argon ions increases. Considering that conductance measured using LCAFM is not a strictly surface quality, as is probes greater volumes than KPFM, we can assume that with surfaces sputtered with ions of higher energy would be more conductive (as is the case, as you can see in Figure S3 in Supplementary Information). Concerning following annealing, and cycles in general, it can be deduced that the surface stoichiometry would be restored and therefore the work function would reach the same values as shown on the Fig. 5, but in the case of conductivity the ion energy would impact the end values.

The following annealing fully changes the surface – both its morphology and electronic properties. After annealing, the surface is composed of atomically-flat terraces (Fig. 5b) with long-range ordering (as reflected in the LEED (1 × 1) pattern). The XPS spectrum (Fig. 5d) shows a spectrum that corresponds to the stoichiometric spectrum.

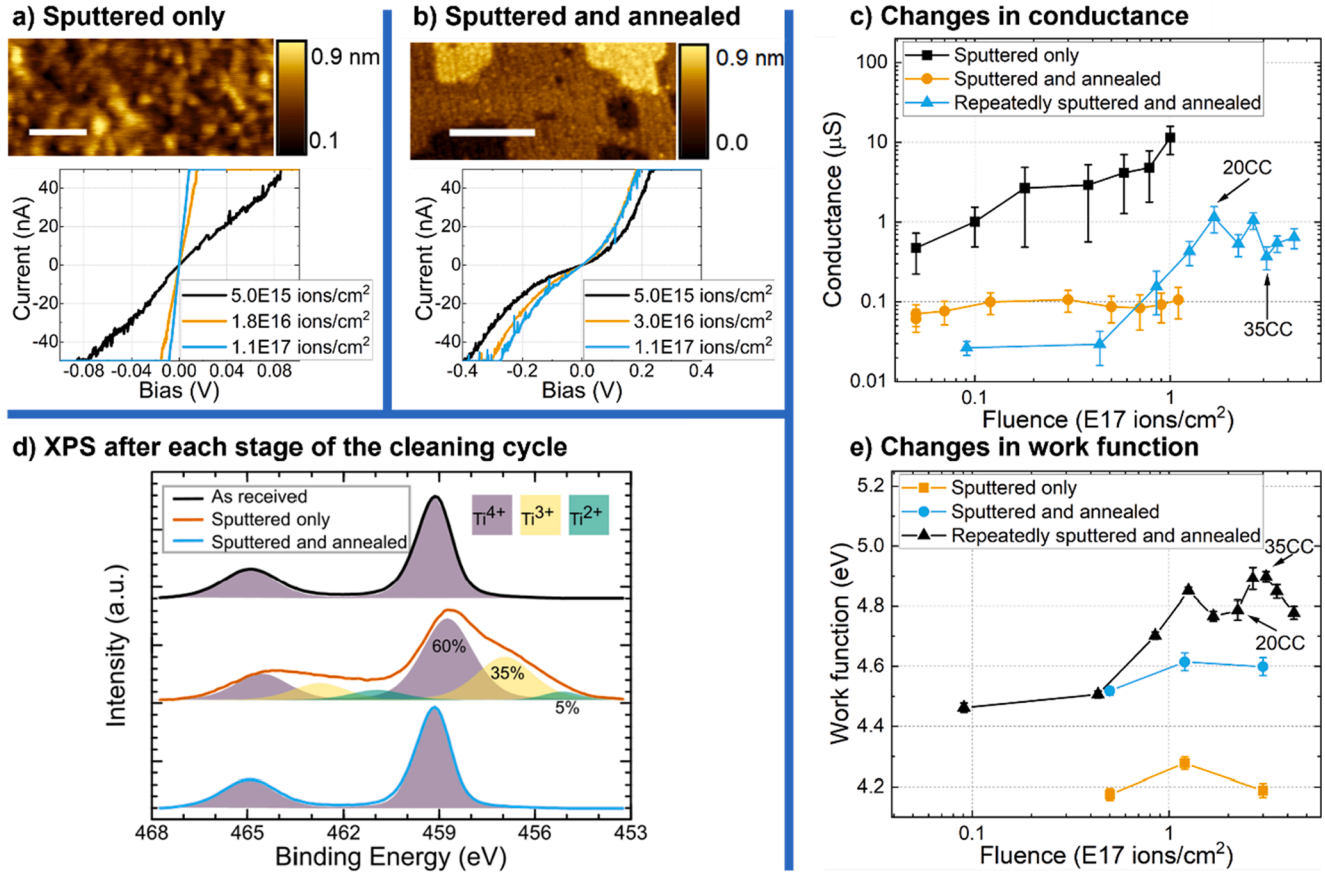

Fig. 5. The TiO_2(1 1 0) topography of: a) sputtered (AFM map, scale bar 100 nm, fluence: 1.0E17); and b) the sample sputtered and annealed at 800 °C (STM image, scale bar: 30 nm). The changes in the conductance and work function, depending on the ion-beam fluence and sample preparation conditions, are shown in c) and e), respectively. d) shows the XPS spectra of the TiO_2(1 1 0) surface during both parts of the CC as compared to the degassed-only sample. Based on the XPS peak fitting, the relative concentrations of 4+, 3 + and 2 + ions are in proportion to approximately 60%, 35% and 5% after the sputtering step, whereas after the successive annealing step, only 4 + is detectable.

Naturally, this then leads to changes in the electronic properties. The surface conductivity reverts to approximately the same value, regardless of the fluence (Fig. 5c), and the I-V curves display a semiconductor-like shape (Fig. 5b). After annealing, the work function drastically increases, which is most likely caused by the return of the crystallographic order on the surface, as well as its stoichiometry (and therefore the reduced number of surface defects, as revealed by the XPS spectra in Fig. 5d).

4. Discussion

As presented in the experiments outlined above, the final physicochemical properties of the atomically-flat TiO_2(1 1 0) surface depend on the way in which is prepared. Preparation based on sputtering and annealing processes leads to a stoichiometric TiO_2(1 1 0) surface of different work functions and electrical conductivity levels, depending on whether the sample received the same ion-beam fluence in one step or multiple ones.

After sufficient sputtering time, the ion beam irradiation of TiO_2(1 1 0) by preferential oxygen sputtering yields a Ti-enriched surface with a saturated chemical composition [25]. The surface dramatically changes during the sputtering process, with the XPS spectra showing that 35% of the titanium is in the + 3 and 5% in the + 2 oxidation states. Thus, the sputtered surface cannot be described as the TiO_2 surface, as such a large proportion of the titanium is not in the + 4 oxidation state. This is supported by the literature, in which it has been reported that ion sputtering, with ion beam fluences similar to the present study, lead to the formation of the Ti_2O_3 phase [71] or even TiO [60]. Furthermore, the sputtered surface does not exhibit the long range ordering of LEED images. This could mean that the surface is highly disordered, or that it is composed of small crystallites that have sizes below the coherence of the electron beam, and therefore do not form diffraction spots. We believe that the crystallites of various sub-stoichiometric titanium oxide phases form in accordance with the principle of aggregation of the point defects into extended defects, and finally different phases, as has been shown elsewhere [30].

The following annealing process changes the state of the surface, as with increased temperature the flow of oxygen from the bulk is possible, which restores the surface stoichiometry. Nonetheless, the restoration of the surface's stoichiometry occurs at a cost of further reduction of the crystal as a whole, with a gradient of non-stoichiometry in bulk from the higher non-stoichiometry closer to the surface and reaching stoichiometry in the bulk [72]. It has been shown with thermogravimetric measurements that even a reduction in temperature of 800 °C causes oxygen losses that would lead to structural changes in the crystal [30]. Thus, even though the surface stoichiometry is restored during annealing (as depicted in our XPS spectra and LEED images), the bulk and subsurface are not perfect and stoichiometric, but defective in a significant manner, as not only the surface properties change (such as the work function and conductivity) but also the crystal macroscopically, for instance the color of the crystal changes. In short, in the combined processes of bombardment and subsequent annealing, a modified TiO_{2-x} layer several tens of microns-thick is formed [30], whereas the interior of the crystal remains unchanged.

The processing of TiO_2(1 1 0) by either an ion-beam fluence in a single or multistep manner, as depicted in Fig. 5e, affects the surfaces of different properties. The values of the work function and conductivity are approximately the same for an initial stage of multiple CCs and a single CC of the same fluence. However, the divergence for higher fluences between the values for samples that received the same fluence in one step or multiple ones is clearly seen for a greater number of such cycles. The work function and conductivity for multiple cycles are larger for a multistep sample than an equivalent single cycle. These differences stem from the fact that the reduction in the crystal occurs in a different manner for both cases. For a single cycle, during sputtering, the reduction of the crystal, as measured by the percentage of titanium + 3 and + 2 ions, will initially cause a lot of oxygen to be removed. However, a plateau is later reached in which the sputtering of oxygen is not as efficient as previously. An equilibrium is reached between the sputtering of titanium and oxygen, and no further changes in stoichiometry occur, regardless of the sputtering time [25]. However, for multiple small-fluence cycles, the situation is different, as in between the sputtering phases, annealing occurs, which brings oxygen back to the surface. Thus, each sputtering process starts from a restored TiO_2 surface, and therefore for multiple cycles, altogether more oxygen is removed from the crystal than compared to the case of the single cycle of equivalent fluence. In other words, the initial stages of stoichiometric TiO_2 sputtering exhibit the largest stoichiometric changes. This seemingly small difference between single-step and multi-step methods leads to differences in the reduction of the crystal, as the small additional non-stoichiometries for cycles will accumulate in the bulk as the number of cycles. Thus, in both cases, annealing will restore the surface stoichiometry, but as the level of reduction of the crystal will differ, the surface properties also will.

5. Conclusions

To conclude, we have shown that the time-tested method of repeated sputtering and annealing does, in fact, restore the stoichiometric TiO_2(1 1 0) surface, but at the cost of significantly altering its electronic properties. The surface remains stoichiometric, but the subsurface region is changed. Even though the LEED images exhibit perfect diffraction patters and XPS measurements indicate a stoichiometric surface, our LC-AFM and KPFM measurements clearly show that the modifications to the subsurface region drastically affect the electronic properties of the surface. We have shown that the final state of the subsurface region is defined by the various intensities of defect migration during the annealing and cooling processes, which are dependent on various chemical gradients caused by the sputtering process. Thus, the properties of surfaces prepared using multiple cycles and singe cycles significantly differ. Using the results presented in this work, the physical processes of sputtering, annealing and exposure to oxygen may be used to alter and tailor the electronic properties, depending on the desired outcome. This is of utmost importance, as conductivity and the work function affect the performance of photocatalytic devices, solar cells and sensors. Furthermore, this work clearly demonstrates that the preparation method of a surface is vitally important to the results of experiments, as it greatly affects the properties and therefore should be thoroughly described in the literature in order to further understanding, as well as make reproducibility easier.

CRediT authorship contribution statement

K. Cieślik: Investigation, Formal analysis, Writing – original draft. **D. Wrana:** Investigation, Formal analysis, Writing – review & editing. **K. Szajna:** Investigation, Writing – review & editing. **W. Bełza:** Investigation, Writing – review & editing. **M. Rogala:** Investigation, Writing – review & editing. **C. Rodenbücher:** Writing – review & editing. **P. Dąbczyński:** Investigation, Writing – review & editing. **K. Szot:** Writing – review & editing. **F. Krok:** Writing – review & editing, Supervision, Project administration.

Declaration of Competing Interest

The authors declare that they have no known competing financial interests or personal relationships that could have appeared to influence the work reported in this paper.

Acknowledgements

Support by the Polish National Science Center UMO-2018/29/B/ST5/01406 and the SciMat Priority Research Area budget (N17/MNS/SCIMAT/2020) under the Strategic Programme Excellence Initiative at

the Jagiellonian University is gratefully acknowledged. M.R. additionally acknowledges the support from the Polish National Science Center – UMO-2016/21/D/ST3/00955. We would also like to thank Christopher Wood for proofreading the manuscript.

Appendix A. Supplementary data

Supplementary data to this article can be found online at https://doi.org/10.1016/j.apsusc.2021.151303.

References

[1] A. Miyoshi, S. Nishioka, K. Maeda, Water Splitting on Rutile TiO2-Based Photocatalysts, Chem. - A Eur. J. 24 (69) (2018) 18204–18219, https://doi.org/10.1002/chem.201800799.
[2] A.A. Haidry, A. Ebach-Stahl, B. Saruhan, Effect of Pt/TiO2 interface on room temperature hydrogen sensing performance of memristor type Pt/TiO2/Pt structure, Sensors Actuators, B Chem. 253 (2017) 1043–1054, https://doi.org/10.1016/j.snb.2017.06.159.
[3] A. Panepinto, et al., Synthesis of Anatase (Core)/Rutile (Shell) Nanostructured TiO2 Thin Films by Magnetron Sputtering Methods for Dye-Sensitized Solar Cell Applications, ACS Appl. Energy Mater. 3 (1) (2020) 759–767, https://doi.org/10.1021/acsaem.9b01910.
[4] J.H. Ri, S. Wu, J. Jin, T. Peng, B. Kim, K.S. Sonu, Preparation of Ti foil-based TiO 2 film containing rutile sea urchin-like microspheres covered with anatase nanotubes self-organized layer and its application in dye-sensitized solar cells, Electrochim. Acta 247 (2017) 754–763, https://doi.org/10.1016/j.electacta.2017.07.035.
[5] S. A. Hamdan, I. M. Ibrahim, and I. M. Ali, "COMPARISON OF ANATASE AND RUTILE TiO 2 NANOSTRUCTURE FOR GAS SENSING APPLICATION," vol. 15, no. 4, pp. 1001–1008, 2020.
[6] S. Mondal Gyanan, A. Kumar, Tunable dielectric properties of TiO2 thin film based MOS systems for application in microelectronics, Superlattices Microstruct. 100 (2016) 876–885, https://doi.org/10.1016/j.spmi.2016.10.054.
[7] N. Becenen, Ö. Altun, Applications of TiO2, ZnO and Ag nanomaterials to denim fabric, J. Nanosci. Nanotechnol. 16 (5) (2016) 5359–5363, https://doi.org/10.1166/jnn.2016.12650.
[8] M.A. Henderson, A surface science perspective on TiO2 photocatalysis, Surf. Sci. Rep. 66 (6–7) (2011) 185–297, https://doi.org/10.1016/j.surfrep.2011.01.001.
[9] M. Bowker and R. A. Bennett, "Erratum: The role of Ti3+ interstitials in TiO2(110) reduction and oxidation (Journal of Physics Condensed Matter (2009) 21 (474224))," J. Phys. Condens. Matter, vol. 22, no. 5, 2010, doi: 10.1088/0953-8984/22/5/059801.
[10] M. Setvin, J. Hulva, G.S. Parkinson, M. Schmid, U. Diebold, Electron transfer between anatase TiO2 and an O2 molecule directly observed by atomic force microscopy, Proc. Natl. Acad. Sci. U. S. A. 114 (13) (2017) E2556–E2562, https://doi.org/10.1073/pnas.1618723114.
[11] D. S. Humphrey, C. L. Pang, Q. Chen, and G. Thornton, "Electron induced nanoscale engineering of rutile TiO2 surfaces," Nanotechnology, vol. 30, no. 2, 2019, doi: 10.1088/1361-6528/aae95b.
[12] Y. Du, N.A. Deskins, Z. Zhang, Z. Dohnalek, M. Dupuis, I. Lyubinetsky, Formation of O adatom pairs and charge transfer upon O2 dissociation on reduced TiO2(110), PCCP 12 (24) (2010) 6337–6344, https://doi.org/10.1039/C000250J.
[13] D. Katsube, S. Ojima, E. Inami, M. Abe, Atomic-resolution imaging of rutile TiO2 (110)-(1 × 2) reconstructed surface by non-contact atomic force microscopy, Beilstein J. Nanotechnol. 11 (110) (2020) 443–449, https://doi.org/10.3762/BJNANO.11.35.
[14] N.G. Petrik, G.A. Kimmel, Electron- and hole-mediated reactions in UV-irradiated O2 adsorbed on reduced rutile TiO2(110), J. Phys. Chem. C 115 (1) (2011) 152–164, https://doi.org/10.1021/jp108909p.
[15] N.G. Petrik, Z. Zhang, Y. Du, Z. Dohnálek, I. Lyubinetsky, G.A. Kimmel, Chemical reactivity of reduced tiO 2(110): the dominant role of surface defects in oxygen chemisorption, J. Phys. Chem. C 113 (28) (2009) 12407–12411, https://doi.org/10.1021/jp901989x.
[16] A. Borodin, M. Reichling, Characterizing TiO2(110) surface states by their work function, PCCP 13 (34) (2011) 15442–15447, https://doi.org/10.1039/c0cp02835e.
[17] C.M. Yim, C.L. Pang, G. Thornton, Oxygen vacancy origin of the surface band-gap state of TiO2(110), Phys. Rev. Lett. 104 (3) (2010) 2–5, https://doi.org/10.1103/PhysRevLett.104.036806.
[18] Y.K. Kim, C.C. Hwang, Photoemission study on the adsorption of ethanol on clean and oxidized rutile TiO2(110)-1 × 1 surfaces, Surf. Sci. 605 (23–24) (2011) 2082–2086, https://doi.org/10.1016/j.susc.2011.08.012.
[19] S. D. Sohn, S. H. Kim, S. K. Kwak, and H. J. Shin, "Defect-associated adsorption of monoethanolamine on TiO 2 (1 1 0): An alternative way to control the work function of oxide electrode," Appl. Surf. Sci., vol. 467–468, no. July 2018, pp. 1213–1218, 2019, doi: 10.1016/j.apsusc.2018.10.233.
[20] C. Zhou, Z. Ma, Z. Ren, X. Mao, D. Dai, X. Yang, Effect of defects on photocatalytic dissociation of methanol on TiO 2(110), Chem. Sci. 2 (10) (2011) 1980–1983, https://doi.org/10.1039/c1sc00249j.
[21] Z. Wu, F. Xiong, Z. Wang, W. Huang, Thermal-, photo- and electron-induced reactivity of hydrogen species on rutile TiO2(110) surface: Role of oxygen vacancy, Chinese Chem. Lett. 29 (6) (2018) 752–756, https://doi.org/10.1016/j.cclet.2018.01.019.
[22] Z. Dohnálek, J. Kim, O. Bondarchuk, J. Mike White, B.D. Kay, Physisorption of N2, O2, and CO on fully oxidized TiO2(110), J. Phys. Chem. B 110 (12) (2006) 6229–6235, https://doi.org/10.1021/jp0564905.
[23] R. Shimizu, K. Iwaya, T. Ohsawa, T. Hasegawa, T. Hashizume, T. Hitosugi, Simplified method to prepare atomically-ordered TiO 2 (1 1 0)-(1 × 1) surfaces with steps and terraces, Appl. Surf. Sci. 257 (11) (2011) 4867–4869, https://doi.org/10.1016/j.apsusc.2010.12.127.
[24] W. Göpel, et al., Surface defects of TiO2(110): A combined XPS, XAES AND ELS study, Surf. Sci. 139 (2–3) (1984) 333–346, https://doi.org/10.1016/0039-6028(84)90054-2.
[25] M. Rogala, Z. Klusek, C. Rodenbücher, R. Waser, K. Szot, Quasi-two-dimensional conducting layer on TiO2 (110) introduced by sputtering as a template for resistive switching, Appl. Phys. Lett. 102 (13) (2013) 1–5, https://doi.org/10.1063/1.4801437.
[26] M. Setvín, et al., Surface preparation of TiO2 anatase (101): Pitfalls and how to avoid them, Surf. Sci. 626 (2014) 61–67, https://doi.org/10.1016/j.susc.2014.04.001.
[27] K. Szot, W. Speier, G. Bihlmayer, R. Waser, Switching the electrical resistance of individual dislocations in single-crystalline SrTiO3, Nat. Mater. 5 (4) (2006) 312–320, https://doi.org/10.1038/nmat1614.
[28] D. Wrana, et al., Tuning the surface structure and conductivity of niobium-doped rutile TiO2 single crystals via thermal reduction, PCCP 19 (45) (2017) 30339–30350, https://doi.org/10.1039/c7cp03136j.
[29] M. Li, et al., The Influence of the Bulk Reduction State on the Surface Structure and Morphology of Rutile TiO2(110) Single Crystals, J. Phys. Chem. B 104 (20) (2000) 4944–4950, https://doi.org/10.1021/jp9943272.
[30] K. Szot, M. Rogala, W. Speier, Z. Klusek, A. Besmehn, and R. Waser, "TiO2 - A prototypical memristive material," Nanotechnology, vol. 22, no. 25, 2011, doi: 10.1088/0957-4484/22/25/254001.
[31] C. Rodenbücher, et al., Local surface conductivity of transition metal oxides mapped with true atomic resolution †, Nanoscale 10 (2018) 11498, https://doi.org/10.1039/c8nr02562b.
[32] E. Arima, H. F. Wen, Y. Naitoh, and Y. J. Li, "KPFM / AFM imaging on TiO 2 (110) surface in O 2 gas," vol. 2, no. 110, 2018.
[33] G.H. Enevoldsen, T. Glatzel, M.C. Christensen, J.V. Lauritsen, F. Besenbacher, Atomic Scale Kelvin Probe Force Microscopy Studies of the Surface Potential Variations on the TiO 2 (110) Surface, Phys. Rev. Lett. 100 (23) (Jun. 2008), 236104, https://doi.org/10.1103/PhysRevLett.100.236104.
[34] W. Melitz et al., "Scanning tunneling spectroscopy and Kelvin probe force microscopy investigation of Fermi energy level pinning mechanism on InAs and InGaAs clean surfaces," J. Appl. Phys., vol. 108, no. 2, 2010, doi: 10.1063/1.3462440.
[35] Z. Kang, et al., Kelvin probe force microscopy for perovskite solar cells, Sci. China Mater. 62 (6) (2019) 776–789, https://doi.org/10.1007/s40843-018-9395-y.
[36] Y. Du et al., "The resistive switching in TiO2 films studied by conductive atomic force microscopy and Kelvin probe force microscopy," AIP Adv., vol. 3, no. 8, 2013, doi: 10.1063/1.4818119.
[37] M.H. Lee, et al., Surface redox induced bipolar switching of transition metal oxide films examined by scanning probe microscopy, Appl. Phys. A Mater. Sci. Process. 102 (4) (2011) 827–834, https://doi.org/10.1007/s00339-011-6266-7.
[38] W. Lu, L.M. Wong, S. Wang, K. Zeng, Probing electrochemically induced resistive switching of TiO2 using SPM techniques, PCCP 19 (46) (2017) 31399–31409, https://doi.org/10.1039/c7cp06992h.
[39] C. Rodenbücher, D. Wrana, P. Meuffels, M. Rogala, F. Krok, and K. Szot, "Electrical nanopatterning of TiO2 single crystal surfaces in situ via local resistance and potential switching," APL Mater., vol. 6, no. 6, 2018, doi: 10.1063/1.5028424.
[40] M. Rogala, G. Bihlmayer, W. Speier, Z. Klusek, C. Rodenbücher, K. Szot, Resistive Switching of a Quasi-Homogeneous Distribution of Filaments Generated at Heat-Treated TiO2 (110)-Surfaces, Adv. Funct. Mater. 25 (40) (2015) 6382–6389, https://doi.org/10.1002/adfm.201500855.
[41] S. Wang, et al., Study on electronic transport properties of WO3/TiO2 nanocrystalline thin films by photoassisted conductive atomic force microscopy, Chem. Phys. Lett. 405 (1–3) (2005) 63–67, https://doi.org/10.1016/j.cplett.2005.01.118.
[42] Y. Du, et al., The resistive switching in TiO2 films studied by conductive atomic force microscopy and Kelvin probe force microscopy, AIP Adv. 3 (8) (2013), https://doi.org/10.1063/1.4818119.
[43] D. Wrana, C. Rodenbücher, W. Bełza, K. Szot, F. Krok, In situ study of redox processes on the surface of SrTiO 3 single crystals, Appl. Surf. Sci. 432 (2018) 46–52, https://doi.org/10.1016/j.apsusc.2017.06.272.
[44] D. Wrana, K. Cieślik, W. Belza, C. Rodenbücher, K. Szot, F. Krok, Kelvin probe force microscopy work function characterization of transition metal oxide crystals under ongoing reduction and oxidation, Beilstein J. Nanotechnol. 10 (2019), https://doi.org/10.3762/bjnano.10.155.
[45] C. Musumeci, A. Liscio, V. Palermo, P. Samorì, Electronic characterization of supramolecular materials at the nanoscale by Conductive Atomic Force and Kelvin Probe Force microscopies, Mater. Today 17 (10) (2014) 504–517, https://doi.org/10.1016/j.mattod.2014.05.010.
[46] E. Sengupta, et al., Photoinduced degradation studies of organic solar cell materials using kelvin probe force and conductive scanning force microscopy, J. Phys. Chem. C 115 (40) (2011) 19994–20001, https://doi.org/10.1021/jp2048713.
[47] S. Kashiwaya, J. Morasch, V. Streibel, T. Toupance, W. Jaegermann, A. Klein, The Work Function of TiO2, Surfaces 1 (1) (2018) 73–89, https://doi.org/10.3390/surfaces1010007.

[48] K. Szot et al., "Influence of dislocations in transition metal oxides on selected physical and chemical properties," Crystals, vol. 8, no. 6, 2018, doi: 10.3390/cryst8060241.
[49] F. Krok, et al., Dynamic force microscopy and Kelvin probe force microscopy of KBr film on InSb(0 0 1) surface at submonolayer coverage, Surf. Sci. vol. 566–568, no. 1–3 PART 1 (2004) 63–67, https://doi.org/10.1016/j.susc.2004.05.023.
[50] H. K. Jeong, C. Yang, B. S. Kim, and K. J. Kim, "Valence band of graphite oxide," Epl, vol. 92, no. 3, 2010, doi: 10.1209/0295-5075/92/37005.
[51] C. Lun Pang, R. Lindsay, G. Thornton, Chemical reactions on rutile TiO2(110), Chem. Soc. Rev. 37 (10) (2008) 2328–2353, https://doi.org/10.1039/b719085a.
[52] H.H. Pieper, et al., Unravelling the atomic structure of cross-linked (1 × 2) TiO 2 (110), PCCP 12 (39) (2010) 12436–12441, https://doi.org/10.1039/c0cp00160k.
[53] "Arbitrary tip orientation in STM simulations: 3D WKB theory and application to W (110) | Enhanced Reader." moz-extension://a1f09f6a-8c08-4905-a980-c0064a92e2b5/enhanced-reader.html?openApp&pdf=https%3A%2F%2Fiopscience.iop.org%2Farticle%2F10.1088%2F0953-8984%2F25%2F44%2F445009%2Fpdf (accessed Apr. 15, 2021).
[54] U. Diebold, "The surface science of titanium dioxide," Surface Science Reports, vol. 48, no. 5–8. Elsevier, pp. 53–229, Jan. 01, 2003, doi: 10.1016/s0167-5729(02)00100-0.
[55] S. Wendt, et al., Oxygen vacancies on TiO2(1 1 0) and their interaction with H2O and O2: A combined high-resolution STM and DFT study, Surf. Sci. 598 (1–3) (2005) 226–245, https://doi.org/10.1016/j.susc.2005.08.041.
[56] F. Rieboldt et al., "Nucleation and growth of Pt nanoparticles on reduced and oxidized rutile TiO2 (110)," J. Chem. Phys., vol. 141, no. 21, 2014, doi: 10.1063/1.4902249.
[57] Z.T. Wang, et al., Probing equilibrium of molecular and deprotonated water on TiO2(110), Proc. Natl. Acad. Sci. U. S. A. 114 (8) (2017) 1801–1805, https://doi.org/10.1073/pnas.1613756114.
[58] Y. Gao, A new secondary ion mass spectrometry technique for III-V semiconductor compounds using the molecular ions CsM+, J. Appl. Phys. 64 (7) (1988) 3760–3762, https://doi.org/10.1063/1.341381.
[59] J. C. Vickerman, "Secondary ion mass spectrometry–basic concepts, instrumental aspects, applications and trends. A. BENNINGHOVEN, F. G. RUDENAUER and H. W. WERNER, Wiley, New York, 1987, 1277 pages," Surf. Interface Anal., vol. 10, no. 8, p. 435, 1987, doi: 10.1002/sia.740100811.
[60] B.M. Pabón, et al., Formation of titanium monoxide (001) single-crystalline thin film induced by ion bombardment of titanium dioxide (110), Nat. Commun. 6 (001) (2015) 1–6, https://doi.org/10.1038/ncomms7147.
[61] M. Rogala, et al., Self-reduction of the native TiO2 (110) surface during cooling after thermal annealing – in-operando investigations, Sci. Rep. 9 (1) (2019) 1–9, https://doi.org/10.1038/s41598-019-48837-3.
[62] K.L. Gilliard, E.G. Seebauer, Manipulation of native point defect behavior in rutile TiO2 via surfaces and extended defects, J. Phys.: Condens. Matter vol. 29, no. 44 (2017) p. aa89ba, https://doi.org/10.1088/1361-648X/aa89ba.
[63] M.A. Henderson, A surface perspective on self-diffusion in rutile TiO2, Surf. Sci. 419 (2–3) (1999) 174–187, https://doi.org/10.1016/S0039-6028(98)00778-X.
[64] K. L. Gilliard-AbdulAziz and E. G. Seebauer, "Elucidating the reaction and diffusion network of oxygen interstitial atoms near a TiO 2 (1 1 0) surface," Appl. Surf. Sci., vol. 470, no. July 2018, pp. 854–860, 2019, doi: 10.1016/j.apsusc.2018.11.123.
[65] P. Gorai, A.G. Hollister, K. Pangan-Okimoto, E.G. Seebauer, Kinetics of oxygen interstitial injection and lattice exchange in rutile TiO2, Appl. Phys. Lett. 104 (19) (2014) 2–6, https://doi.org/10.1063/1.4876916.
[66] J. Yang, L. Li, W. Li, L. Mao, Formation mechanism of conduction path in titanium dioxide with Ti-interstitials-doped: Car-Parrinello molecular dynamics, AIP Conf. Proc. 1794 (January) (2017) 1–7, https://doi.org/10.1063/1.4971906.
[67] S. Wendt, et al., The role of interstitial sites in the Ti3d defect state in the band gap of titania, Science (80-.) 320 (5884) (2008) 1755–1759, https://doi.org/10.1126/science.1159846.
[68] K. Onda, B. Li, H. Petek, Two-photon photoemission spectroscopy of TiO2(110) surfaces modified by defects and O2 or H2O adsorbates, Phys. Rev. B - Condens. Matter Mater. Phys. 70 (4) (2004) 1–11, https://doi.org/10.1103/PhysRevB.70.045415.
[69] A. You, M.A.Y. Be, I. In, "Inverse photoemission study of the defective TiO2 surface.pdf" 2 (February) (1998) 1992.
[70] S. Hashimoto, A. Tanaka, Alteration of Ti 2p XPS spectrum for titanium oxide by low-energy Ar ion bombardment, Surf. Interface Anal. 34 (1) (2002) 262–265, https://doi.org/10.1002/sia.1296.
[71] S. Hashimoto, A. Tanaka, A. Murata, T. Sakurada, Formulation for XPS spectral change of oxides by ion bombardment as a function of sputtering time, Surf. Sci. 556 (1) (2004) 22–32, https://doi.org/10.1016/j.susc.2004.03.002.
[72] K. L. Gilliard and E. G. Seebauer, "Manipulation of native point defect behavior in rutile TiO2 via surfaces and extended defects," J. Phys. Condens. Matter, vol. 29, no. 44, 2017, doi: 10.1088/1361-648X/aa89ba.